RSC Advances

ROYAL SOCIETY OF CHEMISTRY

www.rsc.org/advances

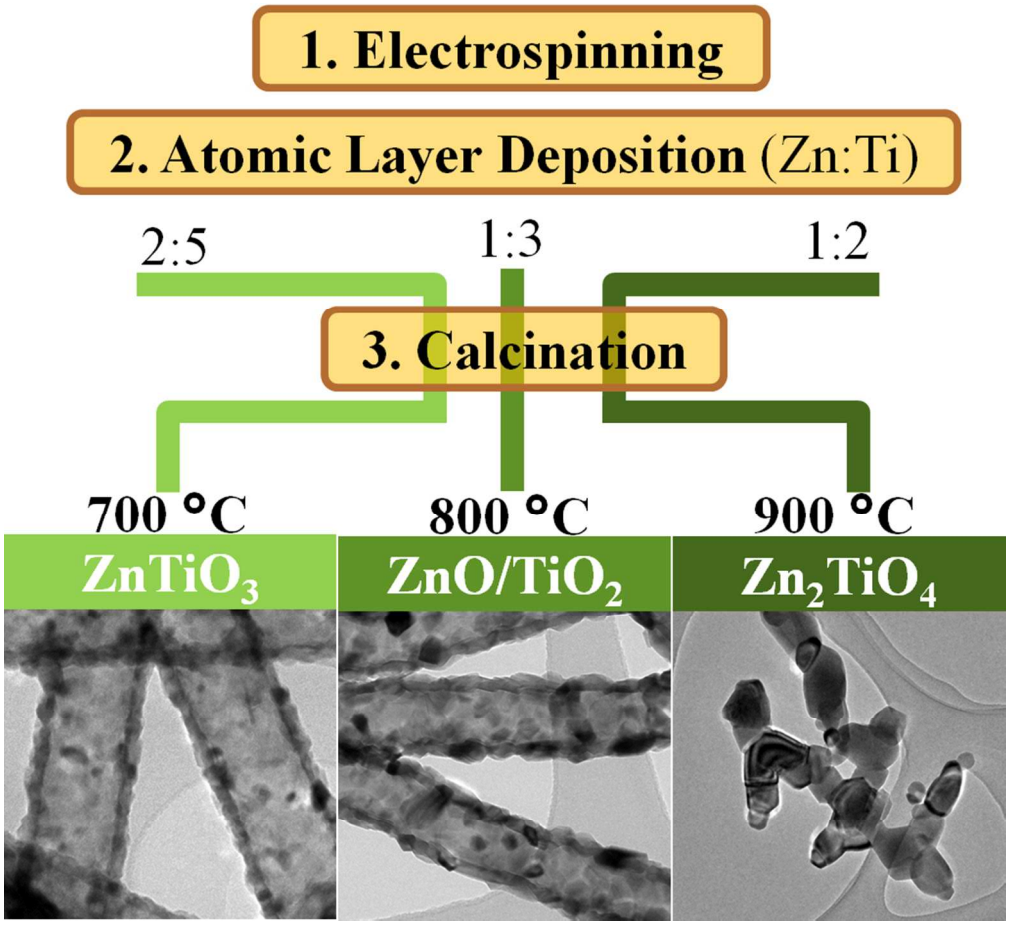

Graphical Abstract

RSC Advances

RSCPublishing

ARTICLE

Surface ionic states and structure of titanate nanotubes

Cite this: DOI: 10.1039/x0xx00000x

Sesha Vempati,*[a] Fatma Kayaci,[a,b] Cagla Ozgit-Akgun,[a,b] Necmi Biyikli,[a,b] and Tamer Uyar *[a,b]

Received 00th October 2013,
Accepted 00th October 2013

DOI: 10.1039/x0xx00000x

www.rsc.org/

Here we present an investigation on Zn-Ti-O ternary nanostructures. Zinc titanates were prepared by a combination of electrospinning and atomic layer deposition. Depending on the ZnO and TiO_2 molar ratio, two titanates and one mix phased compounds were produced by varying the post-annealing temperature. Specifically Zn_2TiO_4, $ZnTiO_3$ and ZnO/TiO_2 nanostructures were fabricated via thermal treatments (900, 700, 800 °C, respectively). Structural studies unveiled the titanate phase of the nanostructures. Furthermore, the chemical nature of the titanate nanostructures on the surface is revealed to be Ti^{3+} and Zn^{2+}. Spin-orbit splitting of Zn2p and Ti2p doublets were, however, not identical for all titanates which vary from 23.09-23.10 eV and 5.67-5.69 eV respectively. Oxygen vacancies are found on the surface of all titanates. The valance band region is analyzed for Zn3d, Ti3p, O2s and O2p and their hybridization, while the edge (below Fermi level) is determined to be at 2.14 eV, 2.00 eV and 1.99 eV for Zn_2TiO_4, $ZnTiO_3$ and ZnO/TiO_2 respectively.

Introduction

Zinc titanates attracted a lot of research attention,[1-6] due to their applicability in microwave dielectrics, catalysts,[1] pigments,[2] lubricant [6,7] and other applications. It should be acknowledged that the formation of titanates through the phase transitions of ZnO-TiO_2 system are relatively complex and of course sensitive to the starting materials and preparation methods.[1,5] It is noted that, for example, the formation of $ZnTiO_3$ is dependent on the initial phase of TiO_2 precursor (anatase TiO_2 produces $ZnTiO_3$) and grain size (larger the grain higher the yield).[5] Some sol-gel methods were established to produce nanoparticles of titanates (see Ref.[1] and references therein, and STab 1 of ESI). Generally, ZnO and TiO_2 are mixed (ball milled for 24h [4] or 2h [5]) in an appropriate stoichiometry and treated at elevated temperatures. In this context atomic layer deposition (ALD) is a very good choice, where $ZnTiO_3$ can be obtained through sequential deposition of ZnO and TiO_2 followed by a regular thermal treatment. Furthermore, ALD can yield complex architectures down to nanoscale with an excellent compositional control and high homogeneity at molecular level [8-12] in contrast to conventional solid-state or sol-gel methods which essentially yield powder or thin films. Layer-by-layer formation of ALD can inhibit the secondary phase formation/segregation during thermal treatments, which is an essential step for the preparation of titanates. Also it can form conformal coatings on complex shapes, high aspect ratio substrates such as nanofibers mats.[10,13-15] By considering these factors it would be very beneficial to investigate the structural details and surface chemical nature of nanotubes. Such investigations are vital in the application point of view, for instance, the catalytic activity depends on the conduction band (CB) edge which in case of titanates is constituted mainly by Ti-centred orbitals. Also, coordination of Ti ions and smaller particle size enhance the catalytic activity.[1,3]

In order to prepare the nanotubes, here, first we have prepared nanofibers via electrospinning which act as template. These nanofibers were subjected to ALD of varying ZnO and TiO_2 molar compositions. These core-shell structured fibers were subjected to calcination of varying though selected temperatures. This procedure has yielded zinc titanate nanotubes, namely, zinc orthotitanate (Zn_2TiO_4), zinc metatitanate (*h*-$ZnTiO_3$) and ZnO/R-TiO_2. These nanostructures were subjected to thorough characterization for their crystal structure and surface chemical composition.

Experimental

Materials: Formic acid (FA, 98-100%) was used as solvents for nylon 6,6. All chemicals were used as received from Sigma Aldrich. Diethylzinc (DEZn) and tetrakis (dimethylamido) titanium (TDMAT) were procured from Sigma Aldrich and HPLC-grade deionized (DI) water was used for the ALD process.

Electrospinning: Uniform and bead-free nylon 6,6 nanofibers were produced via electrospinning. The polymer solution consists of 8 wt.% nylon 6,6 in FA. This mixture was stirred for 3 h at room temperature to obtain a homogeneous and clear solution. This well stirred solution was taken in a syringe fitted with a metallic needle of ~0.8 mm of inner diameter. Then the syringe with solution was fixed horizontally on a syringe pump (KD Scientific, KDS 101) with a feed rate of 1 mL/h. A 15 kV high voltage is applied (Matsusada, AU Series) between the metal needle and a grounded electrode which was kept at a distance of ~10 cm. Grounded electrode was wrapped with an Al-foil to collect the fibers. The electrospinning process was carried out at ~23 ^oC and 36 % relative humidity in an enclosed chamber.

Atomic layer deposition: Supercycles consisting of ZnO and TiO_2 subcycles were deposited on the nanofibers at ~200 °C in a Savannah S100 ALD reactor (Cambridge Nanotech Inc.). N_2 was used as a carrier gas at a flow rate of ~20 sccm. DEZn and H_2O were used at room temperature, whereas TDMAT was heated to ~75 °C and stabilized at this temperature for 30 min prior to the deposition. Depositions were carried out using 'exposure mode' (a trademark of Ultratech/Cambridge Nanotech Inc.) in which dynamic vacuum is

switched to static vacuum just before each precursor pulse by closing the valve between the reaction chamber and the pump. This enables the exposure of precursor molecules to the substrate for a certain period of time (i.e., exposure time). This is followed by a purging period, where the chamber is switched back to dynamic vacuum for purging the excess precursors and gaseous byproducts. Three different samples were prepared using 150 supercycles with different ZnO:TiO_2 subcycle ratios; i.e., 1:2, 2:5 and 1:3. One ZnO subcycle consists of the following steps: valve OFF / H_2O pulse (0.015 s) / exposure (10 s) / valve ON / N_2 purge (10 s) / valve OFF / DEZn pulse (0.015 s) / exposure (10 s) / valve ON / N_2 purge (10 s). One TiO_2 subcycle, consists of the following steps: valve OFF / H_2O pulse (0.015 s) / exposure (10 s) / valve ON / N_2 purge (10 s) / valve OFF / TDMAT pulse (0.1 s) / exposure (10 s) / valve ON / N_2 purge (10 s).

Calcination: Samples of ratios 1:2, 2:5 and 1:3were subjected to calcination at 900 °C (Zn_2TiO_4, ZT14), 700 °C (*h*-$ZnTiO_3$, ZT13) and 800 °C(ZnO/R-TiO_2, ZT12), respectively. These samples will be referred as abbreviated in the parenthesis.

Characterization: The morphologies of the samples were investigated using a Scanning Electron Microscope (SEM, FEI–Quanta 200 FEG). A nominal 5 nm Au/Pd alloy was sputtered onto the samples prior to the observation under SEM. Also transmission electron microscope (TEM, FEI–Tecnai G2 F30) was employed. For TEM imaging, the samples were dispersed in ethanol and the suspension was collected onto a holey carbon coated TEM grid. X-ray diffraction (XRD) patterns were recorded (2θ = 20°- 80°) by employing PANalytical X'Pert Multi Purpose X-ray diffractometer with CuKα radiation (λ = 1.5418 Å). The ionic state of the surface elements were determined via X-ray photoelectron spectroscopy (XPS, Thermo Scientific, K-Alpha, monochromatic AlKα X-ray source, 400 µm spot size, hν = 1486.6 eV) in the presence of a flood gun charge neutralizer. For the core-level spectra, pass energy and step size were 30 eV and 0.1 eV, respectively. Peak deconvolutions of the XPS spectra were performed through Avantage software.

Results and discussion

Schematic diagram of various steps involved to fabricate the nanotubes is shown in Figure 1. Initially polymer nanofibers were produced via electrospinning which were then subjected to ALD of ZnO and TiO_2 subcycles of varying ZnO and TiO_2 content. These core-shell nanofibers were subjected to thermal treatment at 900, 700 or 800 °C yielding three types of nanostructures. i.e. (a) electrospun polymer nanofiber + ALD yields core-shell structure, (b) calcination of (a) at a suitable temperature removes the core polymer and the inorganic coating takes the nanotube form and (c) depending on the calcination temperature a severe reorganization of the crystal structure takes place, then the nanotube structure may collapse yielding grainy fibrous structure.

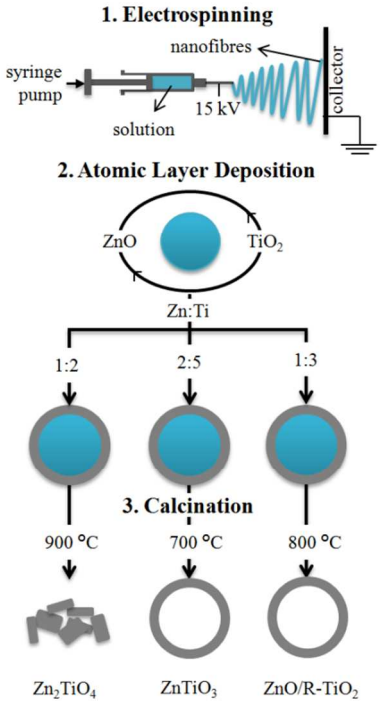

Fig. 1. Schematic diagram depicting electrospinning, ALD and calcination

The representative SEM images of as deposited and calcined samples are shown in Figure 2. The first impression is that the ALD did not cause any deterioration to the polymer nanofibers. After calcination apart from the changes in the crystallinity, morphological changes can be expected [15,16] which is in contrast to the removal of core by washing.[8] From Figure 2a and b these changes are significant and explicit in the case of ZT14 samples which were calcined at 900 °C, where nanotubes are generally expected. In stark contrast, the morphology is completely changed and nanotubes were not seen, however, we can see the traces of fibrous structure with grains. The average diameter and length were 135 ± 12 nm, 175 ± 5 nm and the distributions of which are shown in SFig 1a and b of supplementary information, respectively. The average fiber diameter is about ~90 nm. It appears to be the case that the average diameter of the fiber determines the width of the crystallites while the length is stimulated by the thermodynamics and mobility of the atoms (ions) under high temperature. This excessively high temperature, although required for crystallization, has caused a complete restructuring of the morphology. Since the dielectric properties and the grain size are interconnected [17] the present results are quite interesting as the average diameter of the fiber can be controlled by appropriate choice of the polymer and solvent combination.[10,18] Furthermore, relatively higher diameter (0.5-2 µm) can be achieved by selecting non-polymeric system for electrospinning,[8] which is proven to be compatible in ALD.[8] Notably the uniformity in the grain size reduces the additional dielectric loss.[17] Nevertheless, in XRD we will see the formation of a well developed polycrystalline Zn_2TiO_4. On the other hand, since the ZT13 (Figure 2c and 2d) and ZT12 (Figure 2e and 2f) samples were derived from the calcination at relatively lower temperature, a stark contrast in the morphology is seen. For these samples a nanotube-like structure is evidenced after calcination. To emphasize these samples are similar to those when the core region is subjected washing [8] while keeping aside the changes in the crystallinity due to thermal treatment. It is interesting to see that the nanotubes are thin enough to be electron transparent (Figure 2d and f) where the bottom layer is visible.

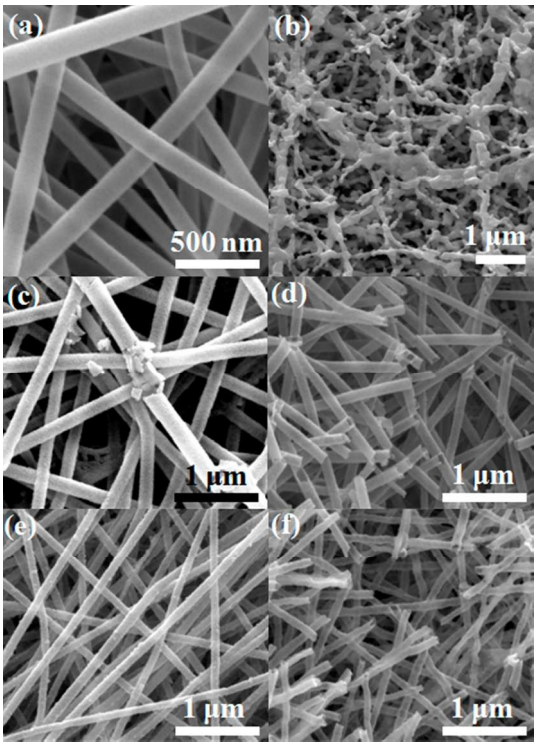

Fig. 2. SEM images of nanotube titanates (a, b) ZT14, (c, d) ZT13 and (e, f) ZT12.

TEM images of titanate samples are shown Figure 3. SEM images of ZT14 have shown a grainy structure, where the expected tubular morphology is lost during the relatively high temperature calcinations (Figure 2b). Hence local crystal structure analysis on ZT14 sample has evidenced well developed crystalline regions (Figure 3a and b). The fast Fourier transform (FFT) image of Figure 3a suggested a single crystalline grain, see insert. Figure 3b suggests a grain boundary region (see the annotations (i) and (ii) on Figure 3b). It is interesting to note that majorly region (i) is polycrystalline in contrast to single crystalline region (ii). Note, as well, we will see that XRD evidenced a polycrystalline nature which averages a large sample unlike TEM. It is generally assumed that the grain boundary region is less crystalline than either of the mating parts. However, this is not the case as we can explicitly see the crystalline grain boundary which obviously is an effect of high temperature calcination. The thickness of the ALD coating is estimated from the TEM images of ZT13 nanotubes and annotated on the Figure 3c and d. ZT13 nanotubes consists of a well developed and uniform sized crystal grains, however the tube like structure sustained its integrity. Furthermore, the diameter of the polymeric nanofiber template, plays an important role in the integrity of the tube with respect to grain size.[8] As mentioned earlier, the uniformity in the grain size is an important character for dielectric properties.[17] ZT12 sample depicted similar character to that of ZT13 sample in terms of grain size uniformity and tube-like structure (Figure 3e and 3f).

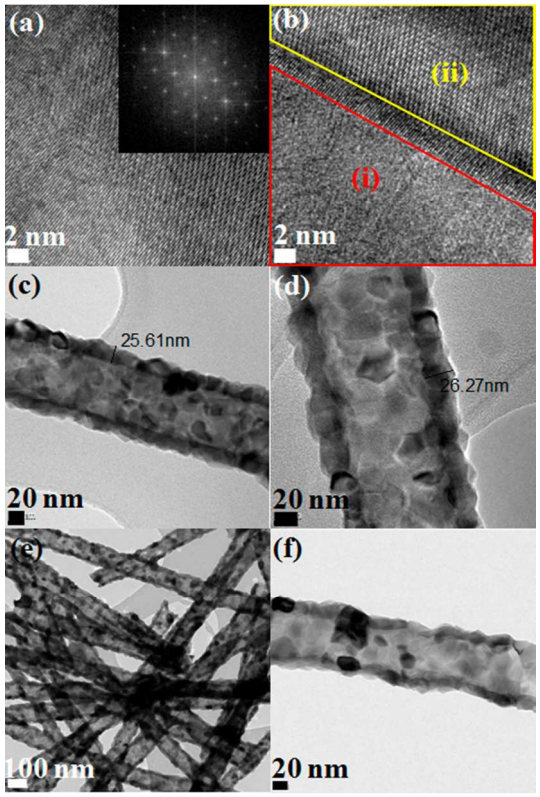

Fig. 3. TEM images of nanotube titanates (a, b) ZT14, (c, d) ZT13 and (e, f) ZT12. Insert of (a) depicts the FFT image of (a) indicating the single crystalline nature.

In Figure 4 we have plotted XRD patterns from ZT14, ZT13 and ZT12 samples along with the identified reflections. In the case of ZT14, it is predominantly cubic (*c*) phased Zn_2TiO_4. When the calcination temperature decreased to 700 °C for ZnO and TiO_2 ratio of 1:2 hexagonal (*h*) phased $ZnTiO_3$ emerged (ZT13). For ZT12 sample we can see the reflections from ZnO and rutile TiO_2 (R-TiO_2) where the calcination temperature is about 800 °C. For this molar ratio, earlier [19] when the calcination temperature increased to 800 °C, *h*-$ZnTiO_3$ and *c*- $ZnTiO_3$ were the dominant phases. Only trace amount of the R-TiO_2 was found.[19] However, in the present context it is notable that for calcination temperatures such as 800 to 900 °C, the *h*-$ZnTiO_3$ is not the dominant phase. At higher temperature the decomposition of *h*-$ZnTiO_3$ into cubic spine (*c*-Zn_2TiO_4) and R-TiO_2 is possible [1,20] and the peaks related to *c*-Zn_2TiO_4 (JCPDS Card No. 25-1164) and R-TiO_2 appeared. For a sample that is treated at 800 °C has shown diffraction pattern of ZnO and R-TiO_2. For the case of *h*-$ZnTiO_3$, (104) and (110) reflections have depicted intensity levels which are the highest and the next highest. Preferential (104) growth orientation is attributed to the reduction in the free energy in reaching a stable growth state. The stable growth state is closed packed plane with lowest surface energy (SE). This is well supported by previous DFT simulations studies. (104) and (110) reflections have shown unrelaxed SE of 5.01 and 5.16 J/m^2 respectively. This SE is decreased ~18% upon relaxation which is a considerable quantity.[6] Furthermore, the FWHM of (104) is about 2θ = ~0.188° in the present case. An earlier ALD grown film [6] has shown relatively higher fwhm of ~1.7° (2θ) which is attributed to growth disorder/defects. i.e. nonuniform strain and/or dislocations, stacking faults and high angle grain boundaries. For instance, stacking faults can be referred to those persist on (104)

plane.[6] Furthermore, these films [6] have depicted condensation of oxygen vacancies (V_Os) (Zn:Ti:O::1:1:2.7) which influences the (104) plane severely such as growth planar stacking faults.[6] i.e. disappearing or introducing an extra (104) plane. Previously,[7] a thin film of $ZnTiO_3$ (ilmenite) depicted only (104) and (12$\bar{}$4) reflections at 2θ = ~33.1° (2.7 Å) and ~62.1° (1.5 Å) respectively. In the present case, these reflections appeared at 32.87°, 62.96°, respectively. This difference can be attributed to the strain due to the nanotube structure, however, note that ref. [7] employs ALD for the synthesis.

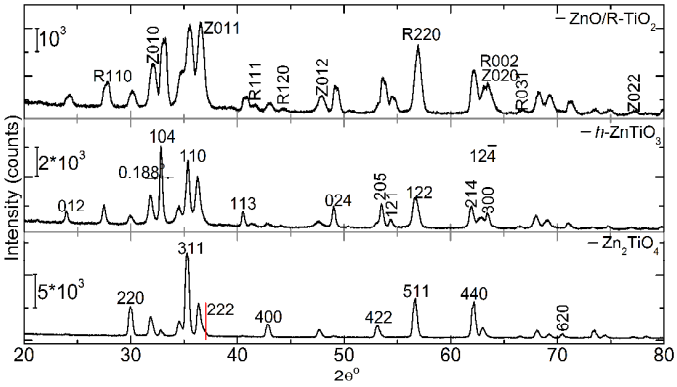

Fig. 4. XRD patterns of nanotube titanates ZT14, ZT13 and ZT12. For ZnO/R-TiO_2 additional planes (104), (110), (113) and (121) from *h*-$ZnTiO_3$ phase were not annotated.

Survey XP spectra for the three compounds are shown in SFig 2 including atomic percentages. The results suggest that the composition of constituting elements is consistent with the chemical formula. However, other phases should be taken into account as we have seen diffraction peaks corresponding to ZnO and R-TiO_2 phases (Figure 4). Carbon contamination might have been occurred during the calcination in ambient atmosphere and subsequent transferring of samples into the XPS chamber. Core-level Zn2p spectra indicated a doublet, $2p_{3/2}$ and $2p_{1/2}$ at ~1021.5 and ~1044.5 eV, respectively, which is indicative of +2 state of Zn. Also two satellite peaks were noticed in the process of deconvolution, however, they were not shown Figure 5. The spin-orbit splitting (ΔE) is ~23.1 eV which is consistent with the literature [21] however the variation can be attributed to the differences in the ionic or covalent environments on the surface. O1s spectra depicted two chemically different environments where the major contribution was due to the lattice oxygen (530.01 eV).[15,21] The other oxygen contribution can be attributed to chemisorbed oxygen (O_{Ch}). O_{Ch} appeared at 531.6 eV indicated incorporation of –OH, –CO, adsorbed H_2O and/or O_2 or O^- and O^{-2} ions [21,22] essentially occupying the V_Os. These defects play a critical role in the emission properties and related applications.[10,15,22] The O_{Ch} contents were 9.76, 8.88 and 7.67 % for ZT14, ZT13 and ZT12 respectively.

Ti2p spectra indicated a single chemical environment in contrast to the samples synthesized by sol-gel technique [1] where Ti2p has two chemical environments for $ZnTiO_3$. The second chemical environment in Ref.[1] is attributed to Ti ions on the external surface of TiO_2 that are partly four or five-coordinated, for particles less than 20 nm. Different reactivities and surface properties are expected from these unsaturated coordination.[23] In the case of TiO_2, the ΔE between $2p_{3/2}$ and $2p_{1/2}$ is ~6.2 eV, where the peaks are at 458.50 and 464.70 eV, respectively. The ΔE for all the samples is ~5.7 eV and attributed to octahedral coordination (Ti^{3+}), although we have seen some XRD reflections corresponding to R-TiO_2. Investigation on local atomic structure has indicated $ZnTiO_3$ and Zn_2TiO_4 have six coordinated Ti^{4+} ions.[4]

Valance band (VB) region with normalized intensity is shown in Figure 5 (bottom). Zn3d is relatively more intense than Ti3p for Zn_2TiO_4 while the converse is true for *h*-$ZnTiO_3$ and ZnO/R-TiO_2 cases. A closure inspection of VB region indicated onset values of −2.14, −2.00 and −1.99 eV for Zn_2TiO_4, *h*-$ZnTiO_3$ and ZnO/R-TiO_2 respectively (Figure 5b bottom right). Upper part of the core-state is occupied by O2s electrons from −19 to −17.3 eV.[21] The VB consists of Zn3d, O2p and Ti3d states. Zn3d state is localized at −5.7 eV, while O2p and Ti3d states hybridize in the range −5 eV to Fermi level (0 eV on the energy scale). However, as we noted earlier, the VB edge slightly differs among the samples which is attributed to the variations in the hybridization of the corresponding orbitals. The results are qualitatively similar to experimental studies about mixed cubic/ hexagonal phase of the compound.[24] To further comment on the band structure, CB composed of Ti3d orbitals. A computed and experimental bandgap of ~3.18 eV [ref [3]] and ~3.1 eV [ref [25]] are evidenced for Zn_2TiO_4, respectively. However, apparently, in the case of spinal structures bandgap depend on the (dis)ordering of the cations at octahedral sites. This essentially implies that the final gap values are strongly influenced by the details of preparation.

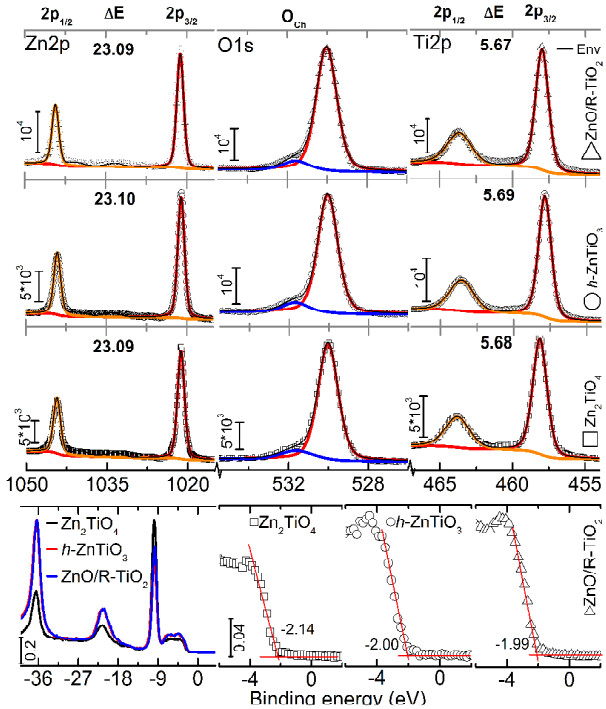

Fig. 5. XP spectra of ZT14, ZT13 and ZT12 samples. In the deconvolution of Zn2p two satellite peaks were present, however, they were hidden in the figure for brevity. 0 eV on energy scale indicate the Fermi level.

Conclusions

Zinc titanate nanotubes were prepared by a combination of electrospinning and ALD followed by high temperature thermal treatment. The crystal structure confirmed the phase formation of *c*-Zn_2TiO_4, *h*-$ZnTiO_3$ and mixed phase ZnO/R-TiO_2. The surface chemical nature of the transition metal ion is determined to be Ti^{3+} and Zn^{2+}. Furthermore V_Os were detected on the surface, however,

with varying O_{Ch} content of 7.67-9.76 %. ΔE of Zn2p and Ti2p doublets was consistent with the literature, while the slight differences are attributed to the environmental effects. The VB edges are determined to be at 2.14 eV, 2.00 eV and 1.99 eV (below Fermi level) for Zn_2TiO_4, $ZnTiO_3$ and ZnO/R-TiO_2 respectively. This study enhances the understanding of the fundamentally important surface chemical nature of titanate nanotubes in addition to the applicability of this process.

Acknowledgements

S.V. thanks TUBITAK (TUBITAK-BIDEB 2221-Fellowships for Visiting Scientists and Scientists on Sabbatical) for the postdoctoral fellowship). F.K. thanks TUBITAK-BIDEB for a PhD scholarship. N.B. thanks EU FP7-Marie Curie-IRG for funding NEMSmart (PIRG05-GA-2009-249196). T.U. thanks EU FP7-Marie Curie-IRG (NANOWEB, PIRG06-GA-2009-256428) and The Turkish Academy of Sciences – Outstanding Young Scientists Award Program (TUBA-GEBIP) for partial funding. Authors thank M. Guler for technical support for TEM analysis. Authors also thank Dr. Z. Ali, Materials Modeling Center, Department of Physics, University of Malakand, Chakdara, Pakistan for providing the computational data of VB and CB for *h*-$ZnTiO_2$ and Zn_2TiO_4.

Notes and references

[a] UNAM-National Nanotechnology Research Centre, Bilkent University, Ankara, 06800, Turkey.
[b] Institute of Materials Science & Nanotechnology, Bilkent University, Ankara, 06800, Turkey.
SV: svempati01@qub.ac.uk; TU: uyar@unam.bilkent.edu.tr

1. Y. Wang, P.-H. Yuan, C.-M. Fan, Y. Wang, G.-Y. Ding and Y.-F. Wang, *Ceram. Int.*, 2012, **38**, 4173-4180.
2. *USA Pat.*
3. Z. Ali, S. Ali, I. Ahmad, I. Khan and H. A. R. Aliabad, *Physica B*, 2013, **420**, 54-57.
4. G. Akgul, *J Mol. Sruct.*, 2013, **1037**, 35-39.
5. Z. Liu, D. Zhou, S. Gong and H. Li, *J. Alloy Compd.*, 2009, **475**, 840-845.
6. W. Sun, A. Ageh, H. Mohseni, T. W. Scharf and J. Du, *Appl. Phys. Lett.*, 2014, **104**, 241903.
7. V. Ageh, H. Mohseni and T. W. Scharf, *Surf. Coat. Technol.*, 2014, **241**, 112.
8. A. Celebioglu, S. Vempati, C.O.-Akgun, N. Biyikli and T. Uyar, *RSC Adv.*, 2014, **4**, 61698.
9. C. O. Akgun, F. Kayaci, S. Vempati, A. Haider, A. Celebioglu, E. Goldenberg, S. Kizir, T. Uyar and N. Biyikli, *J. Mater. Chem. C*, 2015, **3**, 5199.
10. F. Kayaci, S. Vempati, C.O.-Akgun, I. Donmez, N. Biyikli and T. Uyar, *Appl. Catal. B.*, 2015, **176-177**, 646-653.
11. C. O. Akgun, F. Kayaci, I. Donmez, T. Uyar and N. Biyikli, *J. Am. Ceram. Soc.*, 2013, **96**, 916-922.
12. C. O. Akgun, I. Donmez and N. Biyikli, *ECS Trans.*, 2013, **58**, 289-297.
13. P. Heikkilä, T. Hirvikorpi, H. Hilden, J. Sievänen, L. Hyvärinen, A. Harlin and M. Vähä-Nissi, *J. Mater. Sci.*, 2012, **47**, 3607-3612.
14. E. Santala, M. Kemmel, M. Leskela and M. Ritala, *Nanotechnology*, 2009, **20**, 035602.
15. F. Kayaci, S. Vempati, C. Ozgit, I. Donmez, N. Biyikli and T. Uyar, *Nanoscale*, 2014, **6**, 5735.
16. F. Kayaci, S. Vempati, C.O.-Akgun, N. Biyikli and T. Uyar, *Appl. Catal. B.*, 2014, **156-157**, 173-183.
17. R. K. Sirugudu, R. K. M. Vemuri, S. Venkatachalam, A. Gopalakrishnan and S. M. Budaraju, *J. Microw. Power Electromagn. Energy.*, 2011, **45**, 128-136.
18. F. Kayaci, C.O.-Akgun, I. Donmez, N. Biyikli and T. Uyar, *ACS Appl. Mater. Interfaces*, 2012, **4**, 6185-6194.
19. J. Z. Kong, A. D. Li, H. F. Zhai, H. Li, Q. Y. Yan, J. Ma and D. Wu, *J. Hazard. Mater.* , 2009, **171**, 918–923.
20. M. R. Mohammadi and D. J. Fray, *Eur. Ceram. Soc.*, 2010, 947-961.
21. A. V. Naumkin, A.K.-Vass, S. W. Gaarenstroom and C. J. Powell, *Journal*, 2012, **NIST Standard Reference Database 20, Version 4.1**.
22. F. Kayaci, S. Vempati, I. Donmez, N. Biyikli and T. Uyar, *Nanoscale*, 2014, **6**, 10224–10234.
23. T. Rajh, J. M. Nedeljkovic, L. X. Chen, O. Poluektov and M. C. Thurnauer, *J. Phys. Chem. B*, 1999, **103**, 3515-3519.
24. P. K. Jain, D. Kumar, A. Kumar and D. Kaur, *J. Optoelectron. Adv. Mater.*, 2010, **4**, 299.
25. P. H. Borse, C. R. Cho, K. T. Lim, T. E. Hong, E. D. Jeong, J. H. Yoon, S. M. Yu and H. G. Kim, *J. Ceram. Process. Res.*, 2012, **13**, 42-46.